Observation of solar low-l p-modes by the CORONAS–DIFOS experiment

K.-H. Hasler[1], Y.D. Zhugzhda[2], N.I. Lebedev[2], R. Arlt[1], and V.N. Oraevsky[2]

[1] Astrophysikalisches Institut Potsdam, An der Sternwarte 16, D-14482 Potsdam, Germany
[2] Inst. of Terrestrial Magnetism, Ionosphere and Radio Wave Propagation of the Russian Acad. of Sc., Troitsk, Moscow Region, 142092 Russia

Abstract. The CORONAS satellite, launched on 1994 March 2, carried the DIFOS experiment to observe irradiance fluctuations due to global solar oscillations. The DIFOS experiment was working for almost 50 days near solar activity minimum. We present first results of the Fourier analysis of the full time series. The fine structure of the low-l p-modes is shown and fitted with Lorentzian line profiles. Results of the wavelet analysis show strong variations of the p-modes in time.

Key words: Sun: oscillations - Instrumentation: photometers - Methods: data analysis

1. Introduction

The Russian-Ukrainian satellite CORONAS-I (Oraevsky & Zhugzhda 1991) was launched on March 2, 1994 as the first of a new series of solar satellites. Among ten experiments aboard CORONAS-I is the 3-channel full-disk photometer DIFOS, which is aimed to observe global oscillations in the spectral range between 400 and 1100 nm. The intensity measurements are performed with a relative accuracy of about 10^{-5}. The time resolution is 16 s (Oraevsky et al. 1994; Lebedev et al. 1995)

The spacecraft has a circular, quasi-synchronous orbit which allows 20-day periods of continuous observing time every 3 months; the first of such a period without gaps due to the Earth's shadow should have started on May 15, 1994, but the DIFOS experiment was only working until May 7, 1994.

The scientific goals of the experiment are the determination of frequencies, amplitudes and phases of the low-l p-modes in the frequency range 1–10 mHz and the comparison of the measured parameters of the modes with model calculations. An important goal is the observation of the line shapes of the modes caused by stochastic excitations, damping and rotational splitting as well as the variation of the mode-parameters in time. The DIFOS-photometer observes the Sun without any spatial

Send offprint requests to: K.-H. Hasler

resolution. Consequently, it will be only possible to select low-l p-modes with l up to 3.

Doppler shift measurements of velocity fluctuations of solar oscillations have been carried out with high accuracy from the ground for more than two decades. The situation is more complicated for intensity fluctuations because their relative amplitudes are very small. The detection is hampered by the strong atmospheric noise. This problem can be avoided by observations from space (ACRIM aboard SMM, Woodard 1984; IPHIR aboard PHOBOS-2, Fröhlich et al. 1988). We will briefly describe the instrumentation of DIFOS in the following paragraph (see also Lebedev et al. 1995). In Section 2 we will present the frequencies and linewidths resulting from the Fourier analysis. Section 3 contains the results of the time-frequency-analysis (wavelet analysis) of the p-modes.

The 3 channels of the DIFOS photometer are designed for measuring solar irradiance in the following spectral ranges: a) around 550 nm with a band-pass width of 100 nm (glass filter), b) around 750 nm with a band-pass width of 100 nm (glass filter), and c) between 400 and 1100 nm (defined by the spectral characteristics of the silicon photo-diode). Unfortunately, only the last of these channels was working for the full period. The orientation system of the satellite reduces the deviation of pointing the sensors to the Sun below 10 arcmin.

2. Data treatment and Fourier analysis

The time series of the broad-band channel of the DIFOS photometer has a total length of nearly 50 days extending from March 18 through May 7, 1994. It comprises 750 data segments, interrupted by periodic gaps due to the Earth's shadow and a few gaps lasting several orbits caused by malfunctions of the telemetry. The duty cycle is ∼65%. After an extensive treatment of every segment including removal of outliers and filtering slow trends by a polynomial high-pass filtering to reduce the influence of low frequency noise (due to granulation, meso-granulation, and super-granulation), the individual data segments were connected considering their phase. Slow variations were caused by changes in the dark current, temperature drift, changes in the electrical calibration and light scattering.
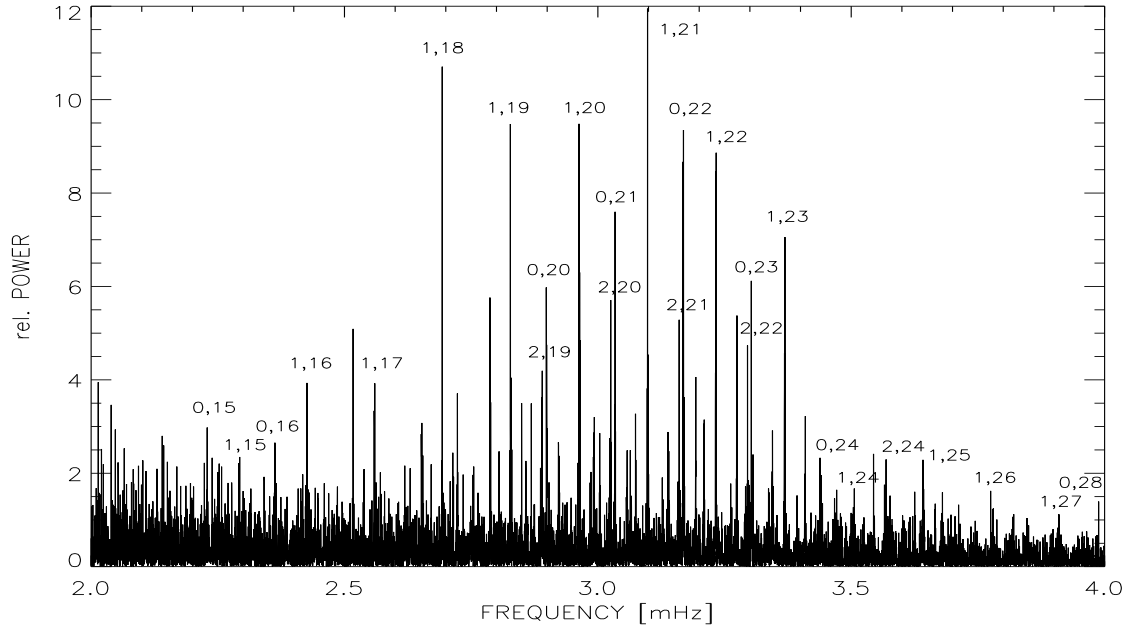
Fig. 1. Power spectrum over the complete observing period. The numbers at the lines give the l and n values of the mode, separated by commas
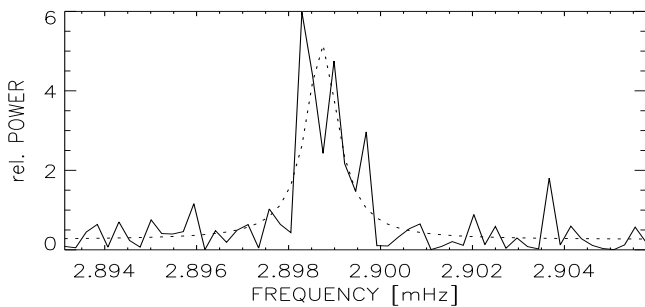

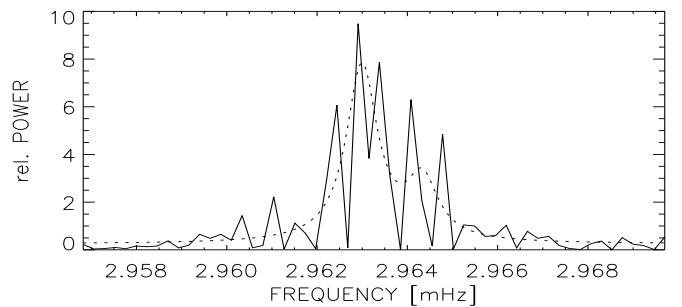**Fig. 2.** Line profile of the $l = 0$, $n = 20$ mode. The dotted line is the maximum likelihood fit

Fig. 3. Line profile of the $l = 1$, $n = 20$ mode. When comparing it with Fig. 2 it seems impossible to distinguish the rotational splitting peaks of $l > 0$ modes and the spurious peaks due to the stochastic excitations. The dotted line is the maximum likelihood fit

The Fourier spectrum of the complete time series is shown in Fig. 1. The frequency resolution is better than 0.3 μHz. Nearly all of the $l = 0$ and $l = 1$ modes in the frequency range of 2.2–4.0 mHz as well as some of the $l = 2$ modes were identified. The other peaks are mainly side-lobes due to the periodic gaps; the revolution frequency of the satellite is 175.6 μHz.

The signal-to-noise ratio (amplitude) of the strongest modes exceeds 3:1. The Fourier spectrum of short periods of two days of the time series also shows the strongest modes, which indicates that the DIFOS data contain a fairly low noise.

The shape of the lines caused by stochastic excitation, damping and rotational splitting can be seen in Figs. 2 and 3. The reason for the rugged line shape is the stochastic excitation of individual modes, which acts as a strong multiplicative noise and will add complex patterns to the peak in the Fourier spectrum. The observed spectrum is the product of the "true" spectrum (a Lorentzian in the case of a single exponentially damped sine wave) and the stochastic source spectrum (Kelly & Ritzwoller 1993). In the case of $l > 0$ modes, this effect is mixed with the rotational splitting into different components.

It is impossible to determine the line parameters, particularly the line width, accurately from these corrupt signals di-

rectly. Therefore, we used a maximum likelihood method to fit the "true" lineshape (assumed as a Lorentzian) and to determine the corresponding line parameters (Toutain & Fröhlich 1992; Toutain & Appourchaux 1994). We assumed different amplitudes for the two visible components of the $l = 1$ modes and fitted a 6-parameter double-Lorentzian to these modes. The observed frequencies listed in Table 1 are in good agreement with other observations for the quiet Sun (Jiménez et al. 1988). The frequencies differ only a few μHz from theoretical calculations (cf. Rüdiger et al. 1997).

Obviously, the acoustic modes cannot be steady with time as they undergo stochastic excitations and damping. The Fourier analysis of the data indeed indicates strong variations of the p-modes in time, which are studied by wavelet transforms in the following section.

3. Wavelet analysis

The temporal variations of the solar oscillations can be analysed by means of wavelet transforms (Bracewell 1965). The

method used in this analysis is a discrete wavelet transform (with a Morlet Wavelet) for evenly sampled data. The parameters of the wavelet transform have to be chosen with respect to the signal characteristics before the analysis. Baudin et al. (1994) calculate the half-width at half height of the windows in the respective domains

$$\Delta T = \frac{1}{\nu}\sqrt{\frac{\ln 2}{a}}, \qquad \Delta\nu = \frac{\nu}{\pi}\sqrt{a\ln 2}. \qquad (1)$$

The central frequency of the wavelet is determined by ν, and a allows us to adjust the width of the window to the value needed.

The very high noise level in helioseismic data and the presence of several close mode frequencies prevent us from using high temporal resolutions. In case of the multi-component modes ($l \geq 1$) the distance between two components is about 0.5 μHz. In order to avoid a significant interference of the components, a frequency resolution of 0.4 μHz is necessary (verified by simulated data). This corresponds to a time resolution of about 6 days.

Table 1. Frequencies of the observed modes derived from the maximum likelihood fit. Linewidths (FWHM) Γ and corresponding lifetimes τ of the observed $l = 0$ modes obtained by fitting a Lorentzian profile using a maximum likelihood method. For comparison the estimated lifetimes τ_w derived from the wavelet anlysis are given. Frequencies ν, σ and Γ are in μHz, τ and τ_w in days.

	$l = 0$					$l = 1, m = 0$	
n	ν	σ	Γ	$\tau = \frac{1}{\Gamma}$	τ_w	ν	σ
15	2229.3	0.60	0.66	17.5	25	2292.6	0.60
16	2362.9	0.55	0.64	18.0	22	2424.8	0.45
17	2495.9	0.50	1.06	10.9	21	2559.2	0.40
18	2629.6	0.45	0.60	19.3	20	2693.7	0.35
19	2763.7	0.40	0.69	16.8	18	2828.2	0.35
20	2898.7	0.35	0.99	11.7	17	2963.7	0.35
21	3033.9	0.35	1.15	10.1	16	3098.6	0.30
22	3168.6	0.35	1.30	8.9	–	3232.8	0.35
23	3303.1	0.40	1.30	8.9	–	3368.7	0.40
24	3438.3	0.55	1.60	7.2	–	3504.9	0.70
25	3576.5	0.70	1.85	6.3	–	3640.6	0.65
26	3712.2	0.80	2.19	5.3	–	3777.8	0.70

We may improve the time resolution for $l = 0$ modes, which have no rotational splitting into components, since the nearest adjacent mode ($l = 2$) is far enough away compared to the resulting frequency resolution. In that case the influence of the noise limits the time resolution to a minimum value of about 2.5 days corresponding to a frequency resolution of 1 μHz. Therefore, the time-frequency analysis will be able to give significant results in both domains if the parameters are suitably optimized.

The time-frequency analysis shows a strong non-steady, independent behavior of the p-modes. The rapid variations in

power occurring in high time-resolution transforms are probably connected to individual excitations. Reasonable results with that time resolution can only be obtained for $l = 0$ modes. A comparison of Fig. 4 with Fig. 2 indicates the correlation of excitations and spurious peaks in the Fourier spectrum.
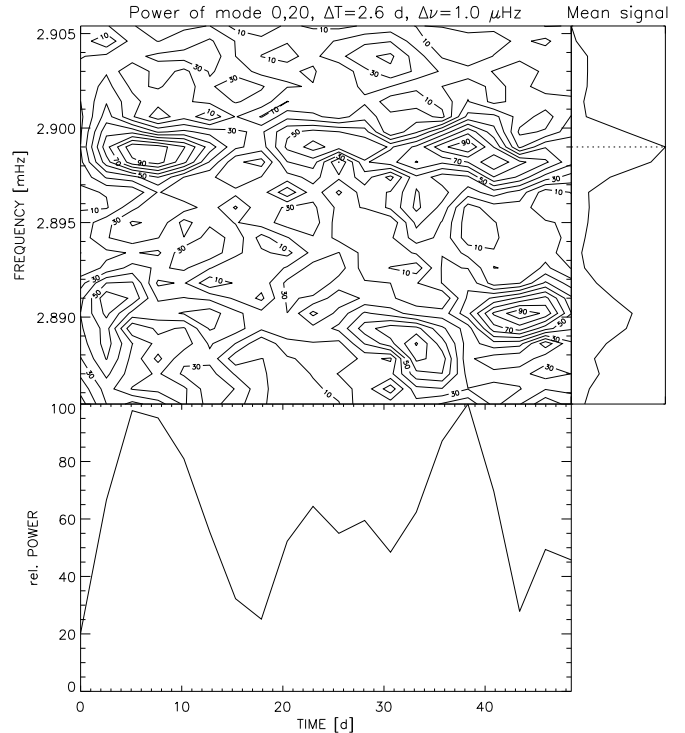

Fig. 4. Wavelet transform of the frequency range of 20 μHz around the $l = 0$, $n = 20$ mode. The contour lines refer to the power; the lower graph shows the power variations of the maximum indicated by a dotted line in the upper graph at the mode frequency. Additionally, the $l = 2$, $n = 19$ mode appears at the lower edge of the contour plot

The raise and decay times seem to be of the same order as the time resolution, particularly for high-frequency modes, but we found that the $1/e$-damping times decrease with the frequency (Table 2). It seems that the lifetimes corresponding to the linewidths are systematically shorter than the lifetimes estimated from the wavelet analysis. This may possibly mean that the lines are not exact Lorentzians. Some modes are easier detectable in the wavelet transform than in the Fourier spectrum of the complete time series, especially if they had been excited only for a short interval of the observation period. The wavelet transform also provides the phase-time information of the modes as the coefficients are complex. The phase shows interruptions during the observing period indicating that the excitations of a mode are independent events.

The energy variations of the $l = 1$ modes show the same non-steady behavior of independent excitations (Fig. 5). Contrary to the Fourier spectrum in Fig. 3, the $m = \pm 1$ components of the mode can be clearly seen. Since the rotation axis of the Sun is perpendicular to the line of sight, the modes with odd $l + m$ values do not appear in the integral sunlight because of a symmetry effect; as a consequence the structure of the $l = 1$

modes must be a doublet, that of the $l = 2$ modes, a triplet. The wavelet transform can even distinguish between stochastic excitation and rotational splitting.

Obviously, the energy variations of the two components of a single $l = 1$ mode are also independent of each other. As shown in Fig. 5 the $m = +1$ and $m = -1$ components of the $l = 1$, $n = 20$ mode are excited at different times. We get a mean rotational frequency splitting $|\nu_{m=0} - \nu_{m=\pm1}|$ of $l = 1$ modes of $0.45 \pm 0.17\ \mu$Hz which agrees well with other observations for the quiet Sun, e.g. Jiménez et al. (1994) who found $0.48\ \mu$Hz.
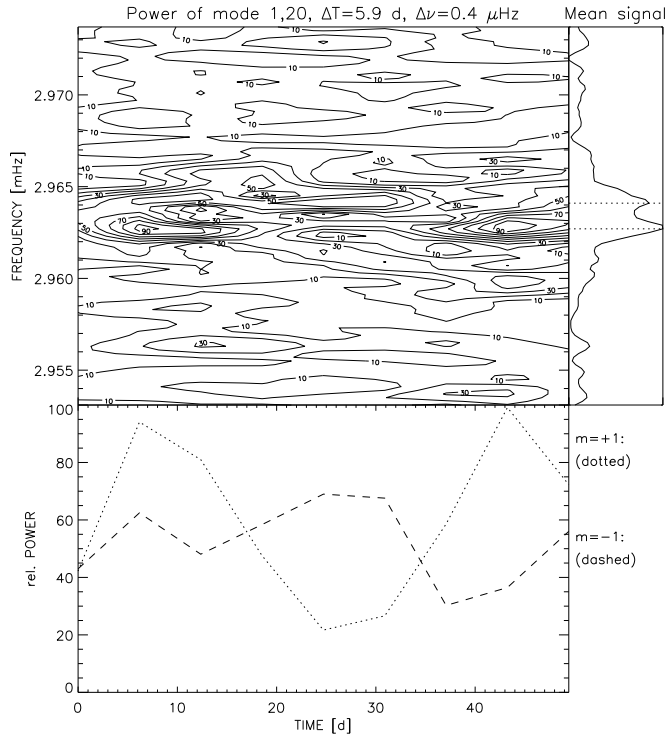

Fig. 5. Wavelet transform of the frequency range of 20 μHz centered on the $l = 1$, $n = 20$ mode. The contour lines refer to the power
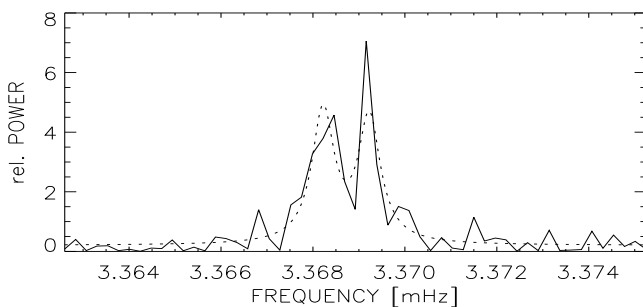

Fig. 6. Fine structure of the $l = 1$, $n = 23$ mode showing both components of the mode. The dotted line is the maximum likelihood fit

The behaviors of the $l = 0$ and $l = 1$ modes resemble those derived from the IPHIR data of the PHOBOS-2 space probe (Baudin 1995). Except the $l = 1$, $n = 23$ mode shows a single "impulsive" excitation during the last 15 days with both components showing the same variation in time. In the remaining

period this mode was quiet. With the information regarding the temporal behaviour of the time series, it can be useful to select an interesting part of the time series, e.g. for Fourier analysis. As an example, the analysis of the $l = 1$, $n = 23$ mode with both components excited during the last 15 days enabled us to select a period for the Fourier spectrum free of stochastic excitations. The better signal-to-noise ratio is striking and the statistics of the mode seems to be less complicated (Fig. 6).

4. Summary

The solar p-modes in the range $n = 15$–28 for $l = 0$, $n = 15$–27 for $l = 1$ and $n = 19$–24 for $l = 2$ were identified. Frequencies and line widths for $l = 0$ and $l = 1$ modes are given as a result of single and double-Lorentzian distribution fits. Damping times of the excited solar p-modes were also derived from wavelet transforms. The wavelet analysis indicates independent temporal behaviour of the rotationally split components of the $l = 1$ modes. This matches the suggestion that the oscillations are randomly excited by the turbulence in the convection zone.

References

Baudin F., 1995, In: ASP Conference Series, Vol. 76, Ulrich R.K., Rhodes E.J. Jr., Däppen W. (eds.), 475

Baudin F., Gabriel A., Gibert D., 1994, A&A 285, L29

Bracewell R.N., 1965, The Fourier Transform and its application, McGraw-Hill, New York

Fröhlich C., Bonnet R.M., Bruns A.V., Delaboudinière J.P., Domingo V., Kotov V.A., Kollath Z., Rashkovsky D.N., Toutain T., Vial J.C., Wehrli Ch., 1988, Seismology of the Sun and Sun-like Stars, ESA SP-286, 359

Jiménez A., Pallé P.L., Pérez J.C., Régulo C., Roca Cortés T., Isaak G.R., McLeod C.P., van der Raay H.B., 1988, In: Advances in Helio- and Asteroseismology, Christensen-Dalsgaard J., Frandsen S. (eds.), Reidel, Dordrecht, 205

Jiménez A., Pérez Hernández F., Claret A., Pallé P.L., Régulo C., Roca Cortés T., 1994, ApJ 435, 874

Kelly J.F., Ritzwoller M.H., 1993, ApJ 418, 476

Lebedev N.I., Oraevsky V.N., Zhugzhda Y.D., Kopaev I.M., Kostyk R.I., Pflug K., Rüdiger G., Staude J., Bettac H.-D., 1995, A&A 296, L25

Oraevsky V.N., Zhugzhda Y.D., 1991, CORONAS Information No. 1

Oraevsky V.N., Zhugzhda Y.D., Kopaev I.M., Lebedev N.I., Pflug K., Rüdiger G., Staude J., Kostyk R.I., Keselman I.G., Osipov S.N., Gumenny A.P., Terletsky M.N., Semesyuk I.V., 1994, CORONAS Information No. 8

Rüdiger G., Kitchatinov L.L., Hasler K.-H., 1997, A&A, in press

Toutain T., Fröhlich C., 1992, A&A 257, 287

Toutain T., Appourchaux T., 1994, A&A 289, 649

Woodard M., 1984, Solar Seismology from Space, R.K. Ulrich (ed.), JPL, Pasadena, 189